Observation of collective inner-shell effects for protons backscattered from the Al(110) surface

P. L. Grande and A. Hentz
Instituto de Física da Universidade Federal do Rio Grande do Sul, Avenida Bento Gonçalves 9500, 91501-970, Porto Alegre, RS, Brazil

G. Schiwietz
Hahn-Meitner-Institut, Abteilung SF4 Glienicker Str. 100, 14109 Berlin, Germany

D. Starodub, E. Garfunkel, and T. Gustafsson
Department of Physics and Astronomy, and Laboratory for Surface Modification, Rutgers University, 136 Frelinghuysen Road, Piscataway, New Jersey 08854-8019, USA
(Received 7 December 2004; published 20 July 2005)

The surface peak of 98-keV protons backscattered from a clean Al (110) surface has been studied in detail for three different scattering geometries. The corresponding energy-loss distributions are asymmetric due to the single and double ionization of the Al inner-shell electrons (L shell). Effects beyond the independent-electron model (inner-shell collective effects) have been observed by using Monte Carlo simulations for the ion ballistic and coupled-channel calculations for the inelastic energy loss. These effects decrease the width by up to 10% for the full width at half maximum. Correspondingly, the low-energy tail of the surface peak is reduced in intensity by more than 30% in the case of a large number of near central collisions as in shadowing and blocking geometries.

DOI: 10.1103/PhysRevA.72.012902 PACS number(s): 34.50.Bw, 34.50.Fa, 61.85.+p, 79.20.Rf

Many aspects of the energy-loss processes of ions in solids are well understood at high projectile energies, but important issues related to the energy loss in the polarization field are still unclear [1]. In particular, for atoms having many electrons in inner shells, there is no clear evidence of the role of collective response and its effect of dressing the projectile interaction. Only for the weakly interacting fast light ions and for valence-band electrons is the polarization field successfully described by means of the dielectric function of the medium [2]. Energy-loss distributions under single-collision conditions have been measured for gases [3–7] as well as for solids [8,9]. For the case of multiple ionization, deviations from the independent-electron model have already been identified [6,7], but an influence of dynamic inner-shell screening is presented here for the first time.

An investigation of the full energy-loss distribution allows for a better understanding of inner-shell collective effects in ion-atom interactions and is a prerequisite for monolayer resolution in ion-beam techniques used for depth profiling such as nuclear reaction analysis (NRA) and medium-energy ion scattering (MEIS) [10]. Measurements in solids under shadowing and blocking conditions involving collisions with very small impact parameters are used in this work to study energy-loss processes involving inner-shell electrons. These conditions are realized in high-precision (resolution and statistics) measurements of the so-called surface peak, a high-energy structure that appears in backscattering experiments for crystalline materials.

Here we report on measurements of the energy-loss distribution of the surface peak for protons impinging along the shadowing directions 0°, 30°, and 60° (ϕ=36°) and being backscattered along the blocking direction of 60° with respect to the normal of clean Al(110). These special scattering geometries have some advantages compared to outgoing random directions. They provide the best scenario for the applicability of advanced atomic-physics models, such as coupled-channel calculations, since solid-state effects are of minor importance due to the large energy transfers involved. Moreover, collective effects due to inner shells are amplified in a sequence of near-central collisions since the energy transfer to inner-shell electrons is enhanced.

In this paper, we apply improved experimental and theoretical methods in order to explicitly extract the influence of the dynamic polarization of inner shells as well as the influence of multi-inner-shell ionization on the energy transfer. Furthermore, we provide a Monte Carlo simulation of the surface peak which goes far beyond a stochastic treatment [11].

The experimental technique has been reported previously [11], and only the salient points are repeated here. The scattering experiments have been performed in a UHV chamber. After mounting into the UHV chamber, the Al(110) crystal was cleaned by several cycles of sputtering with 1.0-keV Ne^+ ions and sequential annealing at 720 K, until a sharp (1×1) low-energy electron diffraction (LEED) pattern could be observed. Here 98-keV protons are scattered on the target and dispersed in energy in a high-resolution toroidal electrostatic analyzer [12]. The incoming beam is aligned with the $[\bar{1}01]$, $[\bar{2}\bar{1}1]$, and $[\bar{1}\bar{1}0]$ directions of Al. The outgoing trajectories are the same for all three geometries (in Fig. 1). The energy spectra of the scattered ions are simultaneously collected in an angular range of 20°, centered about the scattering angles (θ_s) 60°, 90°, and 120°. The measured angular distributions of the surface peak yield are shown in Fig. 1, and the displayed blocking dips correspond directly to specific coordinate-space directions of the atomic lattice as in-

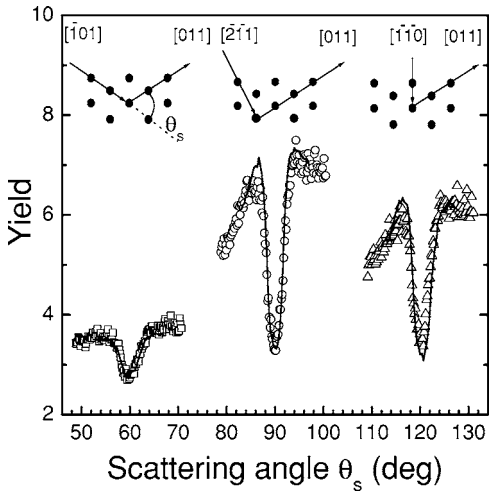

FIG. 1. Surface blocking minima (given in the number of effectively visible monolayers) measured with 98-keV protons in the geometries described in the sketches for three different scattering angles (60°, 90°, and 120°). Lines represent VEGAS [13] simulations from where the structural parameters have been taken [14].

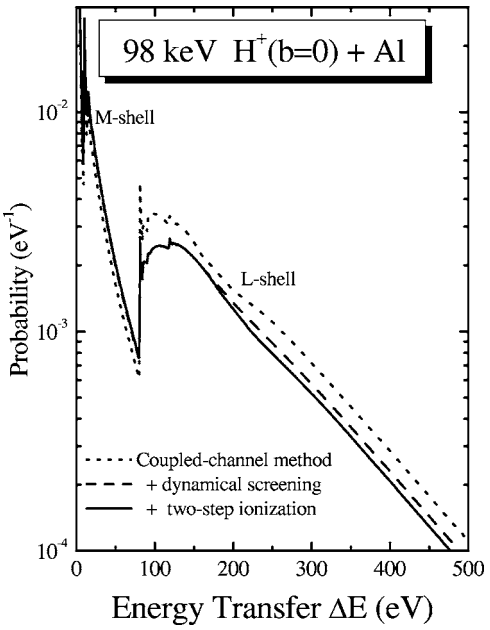

FIG. 2. Energy-loss probability for a single collision with impact parameter close to zero. The dotted line corresponds to coupled-channel calculations without collective effects. Effects beyond IEM are considered as the dashed (including dynamical screening) and solid (including two-step ionization) lines.

dicated for each case. For improved statistics, the energy spectra have been summed up in an angular range of 2° about the blocking minimum position (and corrected by the kinematical factor) to produce the surface peak analyzed below.

The accurate determination of structural parameters (atomic location and vibrational amplitudes) is a usual task in the MEIS technique (see Ref. [14] for the Al surface). This is accomplished by comparing the angular scattering intensity to results of Monte Carlo computer simulations, as implemented, e.g., in the VEGAS [13] code for trial atomic crystal structures (see curves in Fig. 1). This method, however, takes into account only the ballistic part, but not the influence of the electronic energy loss on the backscattering distribution.

In order to describe the energetic shape of the surface peak, we have performed Monte Carlo calculations where the inelastic energy losses are sampled in each collision using the program SILISH (simulation of line shape). It contains the same ballistic part (e.g., determinations of incoming and outgoing trajectories, track connection, interatomic potential, thermal vibrations) as the well established VEGAS program [13]. The electronic energy-loss distribution was calculated through the coupled-channel method [15,16].

Semiclassical coupled-channel calculations are the best tool to describe inner-shell ionization and excitation of atoms [15,16] as a function of the impact parameter. The projectile, following a classical trajectory, provides a time-dependent electrostatic perturbation on the target electrons which is incorporated in a full solution of the time-dependent Schrödinger equation. For a given impact parameter b the amplitudes $a_{i\to f}$ are calculated for any transition from an initial occupied state i to unoccupied bound or continuum states f, and thus the probability corresponding to atomic excitation or ionization is determined. Details of these calculations [atomic orbital (AO)] may be found elsewhere [16].

The independent-electron model (IEM) [18] is adopted for one active electron in the target atom moving in the electrostatic field due to both nuclei and the other electrons, which are included in a frozen-core Hartree-Fock-Slater framework [17]. In this way, the ground-state and excited-state wave functions as well as the energies of the active electron are calculated. Since each excited or continuum state corresponds to a well-defined energy transfer $T=\varepsilon_f-\varepsilon_i$, the electronic energy-loss probability is given by

$$\frac{dP_i}{dT}(b)=\sum_f |a_{i\to f}(b)|^2\delta(T-(\epsilon_f-\epsilon_i)), \tag{1}$$

where the sum above means an integral over ϵ_f, in the case of continuum states.

In the framework of the IEM, the probability for a certain total electronic energy loss ΔE transferred during an individual ion-atom collision can be written as

$$\frac{dP_{atom}^{elec}}{d\Delta E}(b)=\left(\prod_i \int dT_i \frac{dP_i}{dT_i}(b)\right)\delta\left(\Delta E-\sum_i T_i\right), \tag{2}$$

where the index i runs over all electrons for each subshell $1s$, $2s$, $2p$, $3s$, and $3p$ of the Al atom. Equation (2) corresponds to a series of convolutions of individual single-electron energy-loss distributions.

Figure 2 shows the results of the coupled-channel calculations for the energy-loss probability of 98-keV H^+ projectiles colliding with atomic Al at $b=0$. The elastic peak ($\Delta E=0$) is not shown here. The main feature of the energy-loss distributions in Fig. 2 is the significant contribution of the L shell at large energy transfers. The contribution of the valence electrons for the width of the surface peak is of minor

importance since the corresponding M-shell energy loss is much smaller than the experimental resolution. K-shell ionization of Al atoms is kinematically suppressed for protons at incident energies below about 1 MeV. The dotted line in Fig. 2 corresponds to results of the coupled-channel calculations from Eqs. (1) and (2) without any additional correction.

As already noted in [11] the use of such energy-loss probability reproduces the shape of the Al surface peak reasonably well, but important deviations have been found and attributed to the breakdown of the IEM and to the influence of collective effects. The effect of the dynamic modification of the target-electron density leading to a change of the interaction potential (dressed projectile or dynamical screening) and of the reduced probabilities for multiple target ionization are investigated now (Fig. 2).

Using the coupled-channel calculations we can go beyond the independent-electron model by introducing a dynamical screening of the projectile that can be determined self-consistently from the time-dependent electronic density delivered by the coupled-channel calculations. For this purpose we have assumed a dressed potential between the active electron and the projectile described by the Yukawa potential

$$V_p^{dressed} = V_p^{Coul} + V_{ind} = \frac{-\exp(-\alpha|\vec{r}-\vec{R}|)}{|\vec{r}-\vec{R}|}, \qquad (3)$$

where V_p^{Coul} corresponds to the bare (Coulomb) interaction. The constant α has been determined by the induced potential V_{ind} at $\vec{r}=0$ and $t=0$ for each subshell electron ($2s$, $2p_x$, $2p_y$, and $2p_z$) and for each impact parameter. In this way, the influence of the collective screening of the passive electrons on the active one has been estimated. This multielectron iteration procedure leads to a suppression of the energy transfer by about 20% at $b=0$ and corresponds to the dashed line in Fig. 2.

Besides the dynamical screening we have also taken into account the effect of the modification of the target potential after a fast ionization process. According to the IEM the probability, in the case of double ionization, to remove the second electron is equal to the one for the first electron. Here we have adopted instead a sequencial two-step process for double ionization. Instead of using Eq. (2) to describe multi-ionization events we used, for instance, for the energy-loss probability in a double ionization,

$$\left(\frac{dP}{dT}\right)_{double} = \left(\frac{dP}{dT}\right)_{single}(\mathrm{Al}) * \left(\frac{dP}{dT}\right)_{single}(\mathrm{Al}^+), \qquad (4)$$

which corresponds to a convolution of the energy-loss probability with the energy-loss probability in an ionized Al (Al^+) with a hole in the L shell. This corresponds to the so-called two-step ionization model [19], yielding results similar to the average-electron model [6]. For head-on collisions this effect together with dynamical screening is shown in Fig. 2 with solid line. As expected the reduced double-ionization probability (with two L-shell vacancies) due to the collective modification of the target potential affects mainly large energy transfers beyond the summed ionization potential.

The experimental energy distributions for 98-keV incident protons backscattered from a clean Al(110) surface are shown in Fig. 3 (open symbols) in comparison with simulations described previously. The dashed curve corresponds the SILISH simulations using the inelastic energy loss according to the IEM as described by Eq. (2) for the calculations of excitation and ionization of Al as a function of impact parameter (the dotted curve in Fig. 2 for the case $b=0$). The experimental resolution was determined from the leading edge and is about 230 eV (assuming a Gaussian). The agreement between the experimental data and the SILISH simulation is very good for the two larger scattering angles ($\theta_s = 120°$ and 90°). But for the $\theta_s = 60°$ geometry, important deviations can be observed for larger energy losses, as reported in Ref. [11]. The effects concerning the Al (110) structure and the ion collision including all higher-order effects have been very accurately included. Other effects such

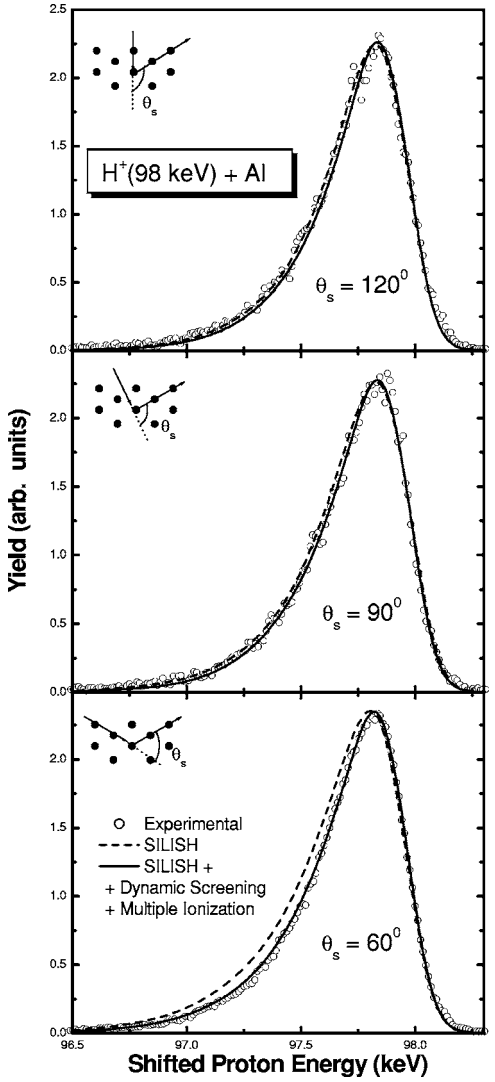

FIG. 3. Experimental data (the open symbols) for 98-keV H^+ backscattered in Al(110) with three geometries (see sketches on each panel). The results are compared to Monte Carlo SILISH simulations. The dotted line corresponds to coupled-channel calculations without collective effects. Effects beyond IEM are considered as the dashed (including dynamical screening) and solid (including two-step ionization) lines. The energy scale for each geometry was shifted to the same leading edge.

as a better description of the valence electrons, dynamic curved ion trajectories, and/or influence of a possible charge state H^0 are of minor importance. In addition, from the simulations we have noticed besides the dominance of the *L*-shell electrons on the energy-loss shape of the surface peak a significant contribution of *double inner-shell ionization* of Al (the triple inner-shell ionization contribution is negligible).

The solid curves in Fig. 3 correspond to the SILISH calculations including collective effects such as dynamical screening and suppressed double ionization due to increased *L*-shell binding according to the procedure explained in Fig. 2. As can be observed, the inclusion of collective effects for the inner-shell electrons is responsible for the deviations and reproduces rather well the experimental data, even for the experimental data at 120° and 90° where the previous agreement with the IEM model was already very good. In fact the $\theta_s=60°$ geometry is distinguished from the others by the number of near-central collisions involved before the backscattering for each layer (e.g., for the fourth layer there are three of such collisions and just one collision for the other geometries). In this way, this particular geometry enhances the effects beyond IEM. This is *evidence for an influence of the dynamic response of inner-shell electrons on the ion energy loss*. It is pointed out that the breakdown of the IEM for the projectile energy loss in multiply ionizing collisions has been recently reported for gases and for highly charged ions. But differently, here a comparable effect is observed even for protons under a special sequence of near-central collisions as in the $\theta_s=60°$ geometry.

In summary, we have observed the influence of inner-shell collective effects such as dynamical screening and target-potential rearrangement in the energy loss of backscattered protons for a special geometry where the number of near-central collisions is maximized. For the other geometries investigated here, however, these effects are barely visible. Thus, the use of the IEM is quite reasonable unless a large number of near-central collisions take place. This fact will be essential for monolayer resolution analytics using the energy loss of ionic projectiles and involving a large number of atoms under shadowing and blocking conditions. It is surprising that collective effects can be important even for protons, and much larger effects are expected for heavier projectiles. This observation has been only possible as a result of the combination of improved energy-loss measurements using a very-well-characterized surface with reliable coupled-channel calculations.

This work was partially supported by the Brazilian agencies CNPq and CAPES, by the program of Brazilian-German cooperation PROBRAL 166/04, and by U.S. National Science Foundation Grant No. DMR-0218406.

[1] G. de M. Azevedo, P. L. Grande, M. Behar, J. F. Dias, and G. Schiwietz, Phys. Rev. Lett. **86**, 1482 (2001).
[2] J. D. Fuhr V. H. Ponce, F. J. Garcia de Abajo, and P. M. Echenique, Phys. Rev. B **57**, 9329 (1998).
[3] V. V. Afrosimov, Y. S. Gordeev, A. M. Polyanschii, and A. P. Shergin, Sov. Phys. JETP **30**, 441 (1970).
[4] C. Auth and H. Winter, Nucl. Instrum. Methods Phys. Res. B **93**, 123 (1994).
[5] R. Schuch, H. Schone, P. D. Miller, H. F. Krause, P. F. Dittner, S. Datz, and R. E. Olsen, Phys. Rev. Lett. **60**, 925 (1988); J. T. Park, Adv. At., Mol., Opt. Phys. **19**, 67 (1983).
[6] M. Schultz, R. Moshammer, W. Schmitt, H. Kollmus, R. Mann, S. Hagmann, R. E. Olson, and J. Ulrich, J. Phys. B **32**, L557 (1999).
[7] B. Skogvall and G. Schiwietz, Phys. Rev. A **46**, 5687 (1992).
[8] W. H. Schulte, B. W. Busch, E. Garfunkel, T. Gustafsoon, G. Schiwietz, and P. L. Grande, Nucl. Instrum. Methods Phys. Res. B **183**, 16 (2001).
[9] Y. Kido, S. Semba, and Y. Hoshino, Nucl. Instrum. Methods Phys. Res. B **219**, 599 (2004).
[10] J. R. Bird and J. S. Williams, *Ion Beam for Material Analysis* (Academic Press, Sydney, Australia, 1989); J. F. Van der Veen, Surf. Sci. Rep. **5**, 199 (1985).
[11] P. L. Grande, A. Hentz, G. Schiwietz, W. H. Schulte, B. W. Busch, D. Starodub, and T. Gustafsson, Phys. Rev. B **69**, 104112 (2004).
[12] R. G. Smeenk, R. M. Tromp, H. H. Kersten, A. J. H. Boerboom, and F. W. Saris, Nucl. Instrum. Methods Phys. Res. **195**, 581 (1982).
[13] J. W. M. Frenken, R. M. Tromp, and J. F. van der Veen, Nucl. Instrum. Methods Phys. Res. B **17**, 334 (1986).
[14] B. W. Busch and T. Gustafsson, Phys. Rev. B **61**, 16097 (2000).
[15] J. F. Reading, T. Bronk, A. L. Ford, L. A. Wehrman, and K. A. Hall, J. Phys. B **30**, L189 (1997).
[16] G. Schiwietz, Phys. Rev. A **42**, 296 (1990); P. L. Grande and G. Schiwietz, *ibid.* **47**, 1119 (1993).
[17] F. Herman and S. Skillmann, *Atomic Structure Calculations* (Prentice-Hall, Englewood Cliffs, NJ, 1963).
[18] M. R. Flannery and K. J. MacCann, Phys. Rev. A **8**, 2915 (1973).
[19] R. Hippler, J. Bossler, and H. O. Lutz, J. Phys. B **17**, 2453 (1984).